Photophysical Processes in Recent Medical Laser Developments: A Review

Article *in* Lasers in Medical Science · August 1986

DOI: 10.1007/BF02030737

CITATIONS
517

READS
409

1 author:

Jean-Luc Boulnois
Babson College
31 PUBLICATIONS **737** CITATIONS

SEE PROFILE

Photophysical Processes in Recent Medical Laser Developments: a Review

JEAN-LUC BOULNOIS
Quantel, BP 23, 91941 Les Ulis-Orsay-Cedex, France

Abstract. A single diagram, encompassing most medical applications for all types of laser in current use, forms the basis of this review of recent medical developments. Emphasis is placed on the physical processes that govern different microscopic mechanisms of laser-tissue interaction. Four distinct photophysical groups are considered in a general classification of these specific modes of interaction: for continuous wave exposure, the photothermal and the photochemical transformations; and, for pulsed irradiations, the electromechanical and the photoablative processes.

The principal photobiological interactions between non-ionizing electromagnetic radiation and living tissues have been extensively reviewed, for radiation in both the submillimetre part of the spectrum and in the optical region (1–7). For laser radiation, the unique characteristic of monochromaticity of the incident field, with the ensuing spatial and temporal coherence of the emission, is finding increasing use in medicine, in both diagnosis and therapy. Together with the biological response of the irradiated tissues, these characteristics determine the *specific modes of interaction* (i.e. the various processes of conversion) of the incident electromagnetic energy within biomolecules.

At present several uncorrelated mechanisms are used in laser photomedicine. The high power densities reached on sub-millimetre spot sizes provide spatially localized heating used in the *thermal* mode of interaction, forming the well known basis of all surgical applications (3–5, 7, 8). The so-called *photochemical* interaction mode, corresponding to the matching of laser frequencies with the specific excitation bands of chromophores, molecules or photosensitizers of precise cellular structures, has recently opened a spectacular field of applications in photodynamic therapy (9–11). The particular combination of temporal coherence in the generation of ultrashort pulses and high peak powers, together with the ability to *focus* laser radiation (spatial coherence) constitutes the essence of the optically induced dielectric breakdown mechanism used in the *electromechanical* mode of interaction (12). The recently introduced techniques of photodecomposition with pulsed ultraviolet lasers (13, 14 and W.S. Grundfest et al, unpublished observations) constitute yet another mode of tissue action, which has been labelled *photoablative* interaction.

This paper reviews the photophysical principles governing these applications. Emphasis is placed on the microscopic mechanisms that control various processes of laser energy conversion. The review starts with the basic observation that these seemingly different interaction modes share a unity (15). Owing to molecular saturation effects, optimal laser parameters associated with a given photomedical process can be arranged into four distinct families that share a single common datum: a total specific energy dose between 10 and 1000 J/cm^2. A single variable distinguishes these processes — namely, the exposure time sufficient for delivery of the foregoing energy dose.

From these findings, I propose to classify the laser-tissue interaction modes into four groups, distinguished by order of increasing time-scale: electromechanical interaction (10 ps to 10 ns pulses); photoablative interaction (10 ns to 100 ns pulses, ultraviolet); thermal interaction (1 ms to 10 s exposure, quasi-continuous wave); and photochemical interaction (10 s to 1000 s, continuous wave).

PHYSICAL PROCESS

Review of the laser photomedical damage chart

Owing to the finite number of individual cells to be treated, whether in chemotherapy or in

Paper received 28 August 1985

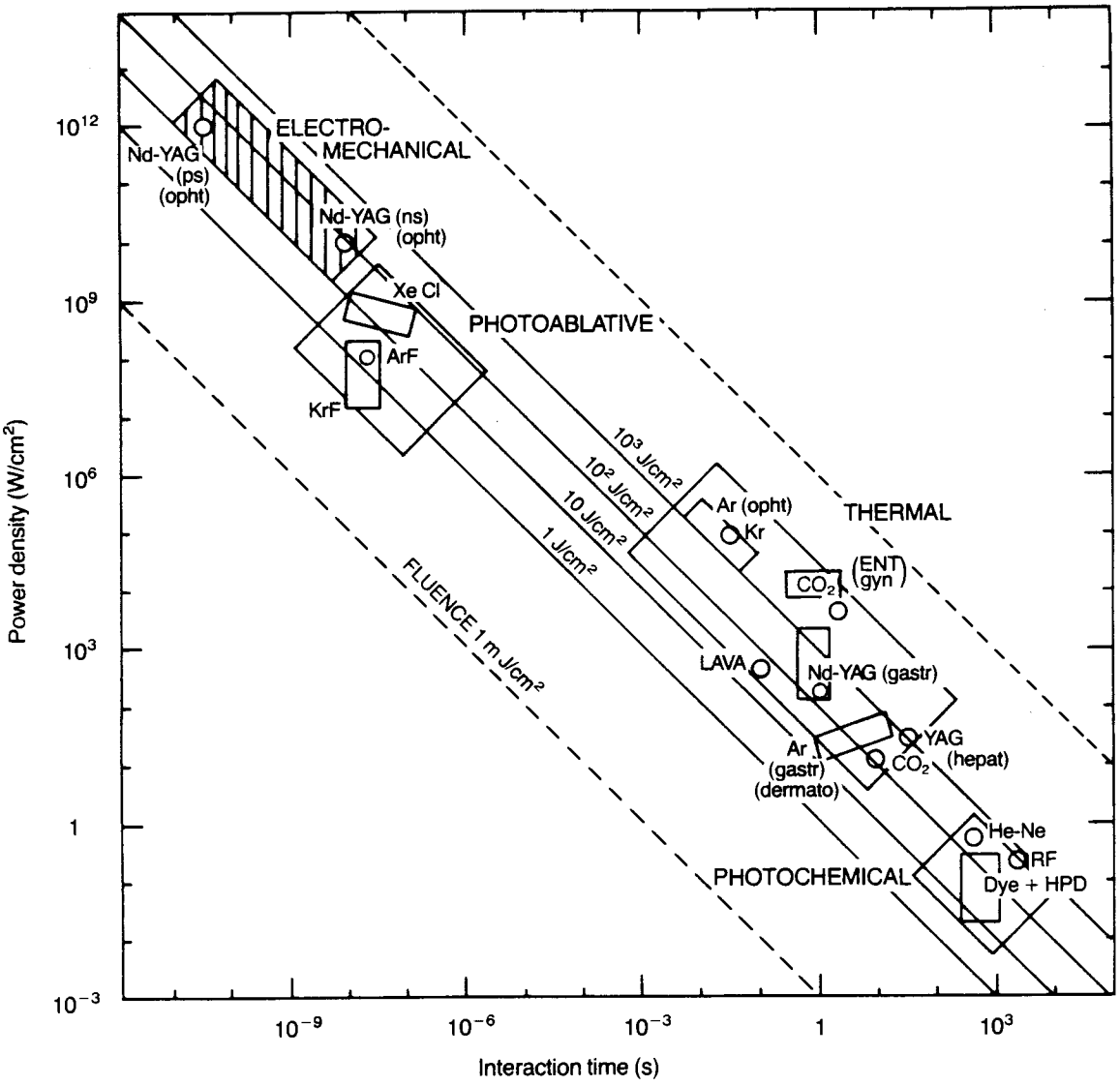

Fig. 1. Medical laser interaction map. The ordinate shows the irradiance (in W/cm^2, on a logarithmic scale), and is commonly labelled the power density. The abscissa shows the interaction time. The diagonals show several lines of constant fluence (in J/cm^2). The boxed areas, labelled electromechanical, photoablative, thermal and photochemical (see text) enclose points that correspond to more than 50 experimentally determined optimal variables obtained from most published reports of clinical and experimental applications of lasers in medicine.

Nd-YAG, neodymium-doped yttrium aluminium garnet laser; XeCl, xenon chloride laser, ArF, argon fluoride laser; KrF, krypton fluoride laser; Ar, argon laser; Kr, krypton laser; CO_2, carbon dioxide laser; Lava, laser-assisted vascular anastomosis; He-Ne, helium-neon laser; HPD, haematoporphyrin derivative. RF, radio frequency; ps, picosecond; ns, nanosecond; opht, ophthalmology; ENT, otorhinolaryngology; gyn, gynaecology; gastr, gastrology; dermato, dermatology; hepat, hepatology.

radiation therapy, the determining parameter is the dose of *reactants* supplied. For an incident radiant flux, the reactants are photons and the energy dose supplied per unit area (the *energy fluence*, measured in J/cm^2) can measure the macroscopic transformation or the 'biological damage' in the general sense (thermal, chemical, mechanical or electrical) caused to the exposed and reacting tissues.

Damage processes in pulsed systems differ from those associated with continuous wave (c.w.) lasers, in that time-constants are substantially different. For c.w. operation, when the pulse time-constant is of the order of the thermal diffusion time or the scattering life-time, damage phenomena are controlled in depth by irreversible thermal effects or chemical transformations. For pulsed operation (picosecond or nanosecond regimes) time-constants are so short that radiant electric-field effects predominate in a zone of extremely small extent.

A chart that gathers together published

information about the medical uses of lasers (15) is shown in Fig. 1. The boxes enclose the points that correspond to more than 50 experimentally determined optimal variables, covering most photomedical applications for a large variety of widely used lasers, such as neodymium-yttrium aluminium garnet, argon, krypton, carbon dioxide, excimer (KrF, ArF, XeCl), and dye or helium-neon lasers. Two major features are displayed on this chart.

First, the data are not scattered uniformly but, rather, are approximately aligned over 12 orders of magnitude on a diagonal within the 10–1000 J/cm^2 fluence band. This reciprocal correlation between intensity and time over a wide range demonstrates that the *specific energy dose* required to achieve a laser-induced biological transformation is *nearly constant*. Consequently, *time* — precisely, the time of exposure during which this energy dose is delivered — appears to be the single parameter distinguishing the transformation process entirely.

Second, four separate groups of transformations, which share this common fluence, can be distinguished, along a diagonal on this chart, according to the duration of interaction: they correspond precisely to the characteristic time-scales of the respective photobiological damage involved.

This distinction into four photomedical families serves as the basis for a classification into four photobiological laser processes that are analysed in this review: the quasi-continuous wave irradiations — thermal and photochemical processes; and the short-pulse regimes — electromechanical and photoablative processes. However, this scheme first requires theoretical confirmation.

At the macroscopic level, to achieve a host response, which might vary with the level of biological organization affected, the laser field should provide a measurable energy dose. Part of this energy dose should be converted within the excited biomolecules, so inducing a 'biological damage' that results, ultimately, in a specific excitation of metabolism. In this two-step modelling, the energy conversion path determines the link between the photophysical step and the biological step in the response.

Microscopically, the photo-induced alteration of individual target macromolecules would then require a finite number of precise energy quanta per molecule, the number being determined by scattering and absorptive properties of the irradiated tissue as well as by the degree of irreversibility of the transformation achieved. Following this approach, a microscopic model based on the foregoing two-step process is proposed, assuming a three-level system (15): first, a resonant absorption at the wavelength corresponding to the incoming photon energy; and secondly, a decay towards the lower excited state, with a subsequent trigger of a biological process and an associated quantum yield. The model establishes that molecular transitions involved in resonant interactions with the laser field should be saturated. It provides a reasonable estimation of the experimental value of the energy fluence shown in Fig. 1; and it clearly shows this energy to be approximately constant and comparable to the *saturation energy* of the excited transitions (15).

In some sense, these findings extend the Bunsen-Roscoe reciprocity law of photochemistry, which states that as long as the product of the irradiance and the time of exposure is the same the photochemical effect will be the same (16). Of course, in exposed biological systems a certain degree of reciprocity failure is to be expected because repair reverses some of the radiation-induced damage (17). This departure from reciprocity should be related to the scatter of the data in Fig. 1 (J.L. Boulnois, unpublished observations).

Thus, the scheme shown in Fig. 1 and the associated microscopic model advantageously reveal the underlying unity between different photomedical laser applications. A general classification of laser-tissue interactions is proposed below, based on the mapping and the time-scale distinction.

Analysis of the different interactions

Thermal interaction

All surgical applications for lasers, whether in cutting or in haemostasis, rely on the conversion of electromagnetic energy into thermal energy. This is achieved through focusing a beam onto spot sizes a few micrometres or millimetres wide: such collimation is possible because of the spatial coherence of lasers which can, hence, supply high densities of energy, providing spatially confined heating of target tissues, which results in thermal injury, tissue removal or control of bleeding. The choice of wavelength and tissue determines the *depth of penetration* and thus influences the interplay between tissue removal and haemostasis.

In fact, a vast majority of therapeutic applications for lasers take advantage of their capability for some spatial control over the degree and extent of tissue injury. The characterization of the photothermal biological response following laser irradiation depends, however, on the structural level at which it is targeted.

At the microscopic level, the photothermal process originates from bulk absorption occurring in molecular vibration–rotation bands or, perhaps, in the vibrational manifold of the lowest electronic excited state, followed by subsequent rapid thermalization through non-radiative decay. The reaction with a target molecule A proceeds in two steps: first, the absorption of a photon of energy, $h\nu$, promoting A to a vibrational excited state A^*; and second, an inelastic scattering with a collisional partner M, belonging to the surrounding medium. On colliding with A^*, M increases its kinetic energy into M′ by carrying away the internal energy released by A^*. The microscopic origin of the temperature rise results from the amount of energy released to M′; the two-step reaction can be schematically represented as:

Absorption: $A + h\nu \longrightarrow A^*$
(vibration–rotation)

Deactivation: $A^* + M(E) \longrightarrow A + M'(E + \Delta E)$

For completeness, it should be mentioned that in normal conditions the kinetic energy per molecule, KT, is about 0.025 eV, while thermal lasers such as carbon dioxide, neodymium-yttrium aluminium garnet (Nd-YAG) and argon have corresponding photon energies between five times larger (CO_2: $\lambda = 10.6\,\mu m$, $e = 0.12$ eV) and 100 times larger (Nd-YAG: $\lambda = 1060$ nm, $e = 1.17$ eV; Ar: $\lambda = 514$ nm, $e = 2.4$ eV). Two factors contribute, then, to thermal efficacy: (a) the rather high probability of deactivation of the excited state A^* which, measured in terms of a *collision cross-section* (18) has values around 10^{-18} cm^2 to 10^{-17} cm^2; and (b) the extremely large number of accessible vibrational states of most biomolecules (10^3 to 10^5): consequently the channels available for de-excitation and thermal conversion are numerous, and the process is highly efficient, provided that the durations of the laser pulses are properly selected.

In contrast to other photobiological laser processes in which the choice of photon energy is usually selected to access a specific reaction channel, the biological effects of heating to first order are non-specific. The scattering and absorption properties of the medium may influence the wavelength selection and, to some extent, the *depth of penetration*; however, the characteristic heating effects are largely controlled by molecular target absorption, essentially from free water, haemoproteins, pigments (e.g. melanin) and other macromolecules such as nucleic acids and aromatics. The photophysical parameter of interest, the absorption coefficient α (cm^{-1}) which measures the *characteristic absorption length*, α^{-1}, is plotted in Fig. 2 over a wide spectral range for several primary elementary biological absorbers (water; oxyhaemoglobin — HbO_2; melanin).

The data are a compendium of properly normalized values (J.L. Boulnois, unpublished observations). Most organic molecules absorb very strongly in the ultraviolet range; water typically reaches 10^6 cm^{-1} in the far u.v. (100 nm). Proteins, which constitute about 15–20% of all cells, also absorb in this spectral region, usually with a peak around 280 nm. Consequently, penetration depths in the u.v. are extremely small (fractions of μm). One notices that HbO_2, predominant in vascularized tissue, also absorbs in other visible bands (green and yellow), but exhibits a cut-off at about 600 nm. By contrast, the absorption spectrum of melanin, the basic pigment of the skin and by far the most important epidermal chromophore, increases monotonically across the visible range towards the u.v. A general feature of most biomolecules is their complex band structures in the high-energy part of the visible spectrum (α ranging from approximately 1 to 10^2 cm^{-1}). Infrared (i.r.) radiation, on the other hand, is absorbed essentially by water with increasingly stronger bands towards longer wavelengths, and typical absorption depths as small as 10 μm in the far i.r. In Fig. 2, a spectral 'therapeutic window' (19) is delineated between 600 nm and 1200 nm: in this range, radiation penetrates tissues with less loss because of weaker scattering and absorption, thereby offering the possibility of reaching deep targets.

The wavelengths corresponding to the most widely used photomedical lasers are also shown in Fig. 2. CO_2 lasers yield immediate vaporization in tissues with a high water content and, hence, they have excellent cutting effects, especially at high power densities (~10 kW/cm^2), producing minimal necrosis but poor haemostasis. By contrast, Nd-YAG laser radiation is capable of deeper penetration, with thermal exchanges taking place in the bulk, and with most of the absorption occurring with

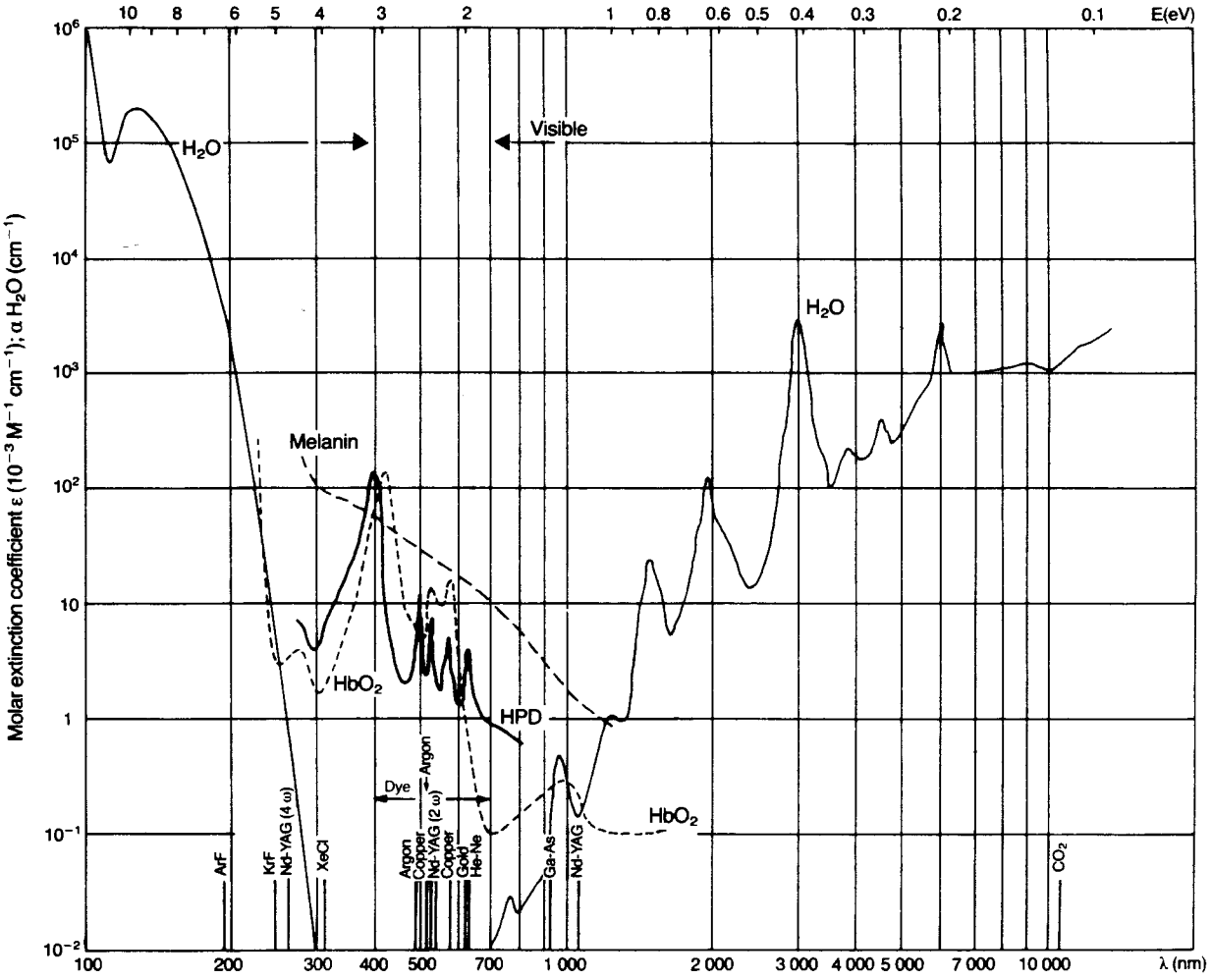

Fig. 2. Absorption coefficient spectrum of water, haemoglobin (HbO_2), melanin and haematoporphyrin derivative (HPD), together with the wavelength positions of the most widely used medical lasers.

hypervascularized and compactly connected tissue (liver tissue, for example, absorbs much more than stomach tissue); the cutting effect is less marked but the haemostatic properties are widely recognized. In the visible spectrum, a host of lasers such as argon, copper, Nd-YAG (second harmonic) or dye lasers show simultaneous interactions with haemoglobin, melanin and other organic compounds, whereas gold lasers fall just outside the HbO_2 absorption cut-off. Dye lasers are attractive since their tunability can be advantageously used to match particular absorption bands of specific chromophores. Being strongly absorbed by haemoglobin, by red globule pigments and by melanin, argon laser radiation is used in subcutaneous vascular coagulations. The u.v. spectral region is fairly well covered by excimer lasers (XeCl, KrF, ArF) which are powerful sources, but the fourth harmonic of the Nd-YAG laser might also prove to be interesting.

The first mechanism by which tissue is thermally affected is by molecular denaturation (of, e.g., proteins, collagen, lipids, haemoglobin). For completeness, Table 1 summarizes the temperature ranges of successive transformations (20).

Table 1. Physical principles of photothermal processes: Conversion of electromagnetic radiation into heat increases the tissue temperature

Temperature	Effects on tissue
43–45°C	Conformational changes
	Retraction
	Hyperthermia (cell mortality)
50°C	Reduction of enzyme activity
60°C	Protein denaturation
	Coagulation
80°C	Collagen denaturation
	Membrane permeabilization
	Carbonization
100°C	Vaporization and ablation

At around 45°C (hyperthermic range) one observes a tissue retraction (or shrinkage) related to macromolecular conformational changes, bond destructions, and membrane alterations. Beyond 60°C is the range of protein denaturation: it results in tissue coagulation which is exploited either to destroy small tumours or to stop haemorrhage (haemostasis). This combination of thermal retraction and haemostasis induces closing of vessel lumens, which can subsequently be obstructed by a blood clot (thrombosis). The temperature limit at which tissues become carbonized is about 80°C. Vaporization occurs beyond 100°C, predominantly from heated free water; the large heat of vaporization of water (2530 J/g) is advantageous, since the steam generated carries away excess heat, thereby preventing any further temperature increase of adjacent tissue. Vaporization together with carbonization yield decomposition of tissue constituents. Laser ablation, which is used to make incisions or resections, serves as the basis of all photosurgical or photocoagulative applications.

These irreversible structural changes reflect tissue thermogenesis caused by deep thermal conduction of the absorbed incident power. The major problem with removal of material is to adjust the duration of laser exposure in order to minimize thermal damage to adjacent zones so as to obtain little necrosis. The scaling parameter for this time-dependent problem is the so-called *thermal relaxation time*, τ, obtained by equating the characteristic absorption length α^{-1} to the characteristic thermal diffusion length, L. This latter quantity is proportional to the square root of time together with a factor involving the tissue diffusivity $\varkappa$ (cm²/s), namely a lumped physical parameter characterizing the material's thermal response (thermal conductivity, specific heat and density). The diffusion length, L, is defined through a relationship of the form:

$$L^2 \sim 4\varkappa t \qquad (1)$$

For example, the diffusivity of liquid water being $\varkappa \sim 1.4\times10^{-3}$ cm²/s, heat diffuses to 0.8 mm in 1 s. From this relationship, one constructs the (wavelength-dependent) relaxation time τ which measures the thermal susceptibility of irradiated tissue:

$$\tau \sim (4\alpha^2\varkappa)^{-1} \qquad (2)$$

For comparison purposes, a summary of thermal relaxation times corresponding to various biological media is presented for several wavelengths of interest in Table 2. Thermal properties are assumed to be those of water (21), whereas collected optical data originate from different published sources (21–23). The respective roles of CO_2 lasers in tissues with a high water content, and of argon lasers in tissues with a high blood content are clearly evident. These data are also consistent with published tissue irradiation times which vary between 1 ms and 1 s, depending on the pigmentation, tissue constituents, width of affected zone and depth of penetration (5).

The water relaxation time at 10.6 μm suggests an interesting operation mode for CO_2 lasers in microsurgery which could be called 'real superpulse mode'. The high temperatures needed for phase change (steam formation), without appreciable heating of adjacent tissues, are reached only when the exposure duration is shorter than τ: consequently, by pulsing the laser with pulses *shorter than 200 μs*, it should be possible to vaporize tissue directly and still obtain an extremely small amount of necrosis. Typical pulses of 10 mJ/50 μs, from a CO_2 laser operating at 50 Hz, would vaporize 300 μm spots and would cut with a velocity larger than 10 mm/s.

In a similar approach, attempts to control tissue temperature for selective photothermolysis (7) have been made recently with a high power Nd-YAG laser (400 W), operating in a repetitively pulsed or burst mode (24); a fast repetition rate (up to 100 Hz) is chosen such that, for a specific tissue with a characteristic cooling rate, a constant average energy is permanently stored in the material: a constant average temp-

Table 2. Thermal relaxation times (in s) for various biological media at wavelengths for different lasers

Biological medium	Ultraviolet (200 nm)	Argon (488 nm/514 nm)	He-Ne (633 nm)	Nd-YAG (1060 nm)	CO_2 (10.6 μm)
Water	30×10^{-6}			20×10^{3}	0.2×10^{-3}
Oxygenated blood	0.2×10^{-3}	15×10^{-3}	9	5	
Plaque		0.5	45	90	
Melanin		0.1	0.5	4	

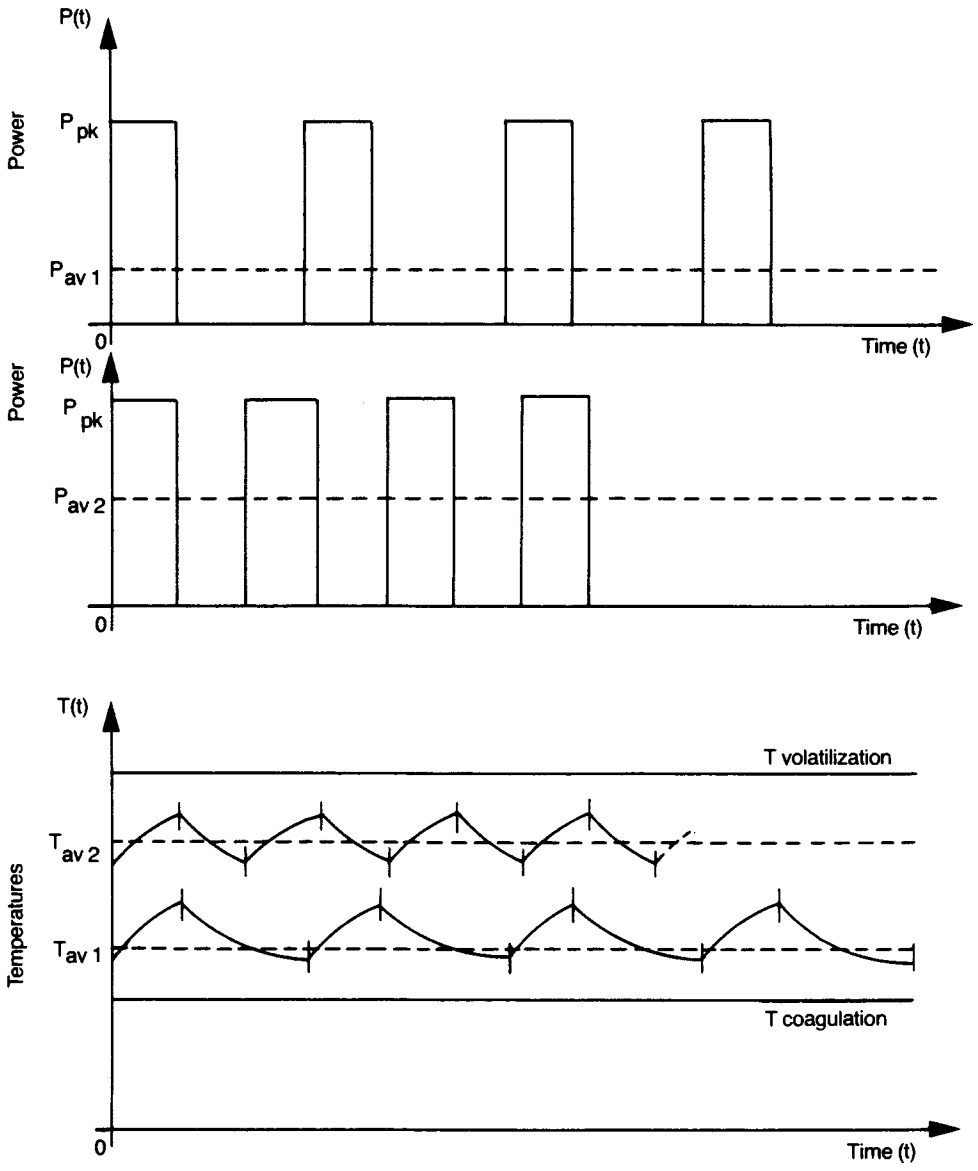

Fig. 3. Scheme showing the temporal control of average tissue temperature T_{av} by adjustment of the repetition rate in a fast-pulsed laser (constant peak power P_{pk}; adjusted average power P_{av}).

erature is thus achieved. By adjustment of the pulse repetition rate, the tissue temperature can be maintained with precision above the coagulation temperature and below the carbonization limit (24). Fig. 3 shows schematically the working principle of this temporal technique, which provides a useful extra degree of freedom to complement current photosurgical methods.

For completeness, I shall now briefly review the well established applications based on photothermal interactions.

In ophthalmology, short interaction times (10–100 ms) are commonly used with argon lasers (1–4 W) or krypton lasers (1–3 W), which are focused on spot sizes of 30–100 μm. This results in power densities up to 10^5 W/cm^2, and brings the local tissue temperature up to around 60 °C. Such processes are typical of the photocoagulation treatment of diabetic retinopathy, retinal detachment (25, 26) or choroidal lesions (27).

Power densities in the range 10^4 W/cm^2 are routinely used with CO_2 lasers for consecutive irradiation pulses of, at most, 1 s each, in laryngeal microsurgery (28, 29) or in gynaecological treatment (30).

Various gastrointestinal bleeding lesions are treated with Nd-YAG lasers operating in the haemostatic mode (31). Resection of various tumours — in gastroenterology, urology, tracheobronchial endoscopy and in general surgery — is usually done with the Nd-YAG, CO_2 or argon

lasers, at typical fluences of 100–1000 J/cm^2 and with corresponding irradiation times of the order of seconds (32–37).

Dermatology is another field in which the argon laser or the copper (510 nm or 578 nm) laser prove useful, particularly for cutaneous coloured lesions or exophytic lesions (38). Selective thermal damage to endogenous tissue chromophores (e.g. haemoglobin or melanin) may induce minimal necrosis to healthy adjacent tissue. This type of subcutaneous vascular coagulation technique, used for treating thrombosis of superficial dysplasia such as portwine stains, requires a careful control of the energy dose with c.w. lasers, to minimize scarring (39). More recently, pulsed copper vapour lasers at 578 nm have been investigated (40) in an operating mode similar to the foregoing 'superpulse mode': pulse duration was about 60 ns (while τ for haemoglobin is about 15 ms) and the energy was around 3 mJ. The process was presumably thermal (possibly via selective heating of blood vessels), owing to the fast deactivation of the HbO_2 excited state and the high average power delivered by such lasers (with repetition rates of ~5 kHz).

Several recent attempts to broaden the scope of existing clinical procedures make use of the thermal effect with new, drastic approaches. Four such developments seem promising.

The first of these is *percutaneous transluminal laser angioplasty*, used in the treatment of thromboembolic and occlusive vascular disorders. One of the main objectives is to obtain disintegration of atheromatous plaques or thrombi with minimal irreversible damage to artery or vessel walls. The technique for removing obstructions (41) was first demonstrated with 4 W argon laser radiation, coupled with a special optical-fibre catheter (42) before being applied to human arteries (43). Although wall perforations have been reported with Nd-YAG systems (44), the role of perfusate absorption has been stressed (45). A newly proposed technique, for coaxial positioning of a fibre-optic balloon catheter within arteries together with a flowing perfusate, has demonstrated that conditions could be found in which no arterial wall perforation or distal embolization took place. Angiograms of femoral arteries in vivo, with 4 mm length and 1 mm internal diameter stenosis, show efficient recanalization after three exposures at 12 W (36 000 J/cm^2 fluence) (46). Owing to the strong interest in these procedures, extensive modelling of thermal and optical interaction with plaques and vessel walls have been proposed recently (23, 21, 47), to predict the threshold laser powers necessary to reach 100 °C at the fibre tip; a recent review has been devoted to the subject (48).

In a related development, extensive interest is currently generated by the use of low-power thermal lasers for vessel welding. *Laser-assisted vascular anastomosis* (LAVA) may become a major procedure in microvascular surgery (49). Although initial repair work on 1 mm vessels was done with Nd-YAG lasers (50), 750 mW argon lasers have been shown to be efficient in coagulating blood to form an adherent tensile sleeve for the anastomosis of small vessels (51). Continuous-wave CO_2 lasers, operating in the range 50–200 mW in a series of short 0.1 s exposure bursts along the anastomotic line, have also recently proved effective (52–54). In an experimental model, rat femoral arteries (0.8–1.2 mm) were exposed at 35 J/cm^2 fluence levels to 150 μm spot sizes: a first brief pass is made around the entire vessel for sealing purposes and a second for supplementing the bond strength (stay sutures were used for adjusting the edges). Sequential histological findings show the appearance of an initial coagulation bond, coapting the edges, followed by a healing process with proliferating intimal cells and neovascularization at the laser anastomotic site over a 2–3 week recovery time. Besides reducing the operating time considerably LAVA, when developed into an established technique, may offer attractive advantages: it seems to perform better seals, with no leakage, in a relatively non-traumatic manner. Potential clinical applications are in reimplantation, tissue transfer, revascularization, circulation improvement, or in other conditions in which sealing of leaking or damaged vessels is necessary.

Waveband interaction is a third barely explored aspect of laser interaction that is currently attracting attention: a synergistic effect is possible when this technique is used for irradiating a biological sample with two monochromatic wavelengths (55). In related clinical investigations, various partial resections of the liver have been done with CO_2 and Nd-YAG lasers in combination (56). In a small series of four patients, successful partial resections of the liver were achieved with a prototype handpiece that combined a focused 60 W CO_2 laser and a defocused 80 W Nd-YAG laser: the necrotic zones were significantly reduced, and defocused Nd-YAG radiation appeared to be an efficient haemostatic tool (57). Similarly, in lung cancer

treatment, bronchial obstructions are first endoscopically cleared with an Nd-YAG laser, and a radioactive irridium wire is subsequently inserted, causing localized necrosis of the neoplastic tissue (58): damage to healthy tissue seems to decrease in this laser–radiation combination. Photosynergism, when extended to other dual wavelengths, could certainly be used in a preconditioning treatment, through a combination of infrared or visible laser exposure together with ionizing radiation, for example, thereby offering great advantages for the treatment of tumours.

The fourth experimental development, flashlamp pumped pulsed dye lasers, emitting in the visible range between 450 and 600 nm and operating at 5–30 Hz repetition rates, are being investigated in conjunction with a fibre delivery system in the *fragmentation of kidney stones*, at fluence levels in the range 20–200 J/cm^2 (40). Short pulses, lasting from 10 to 400 μs, with energies ranging from 10 to 200 mJ, locally heat an extremely small volume of the kidney-stone porous matrix. This heat is rapidly conducted to the interstitial water that is confined inside the matrix microcavities, so bringing it to boiling point: the subsequent pressure rise creates the desired localized fragmentation of the stone. Since the water heat of vaporization is about 2530 J/g, pulses of 250 mJ will heat up a focal volume at most equal to 0.1 mm^3 which, for typical small kidney stones (a few mm in diameter) requires exposure times of tens of seconds before the fragmentation is complete. Besides their cost-effectiveness and their possibility of operating at higher repetition rates, pulsed dye lasers offer a major advantage because their broad emission spectrum covers a large number of absorption bands for the constituents of calculi, which are essentially calcium or magnesium salts of phosphates or oxalates.

Photochemical interaction

At the very end of the exposure scale, for extremely long interaction times (~1000 s) and low power densities (below 1 W/cm^2), lies the family of photochemical transformations. In most instances, the basic physical channels for photochemical interactions between laser radiation and cellular structures are only partially elucidated.

However, within the 'therapeutic window', radiation penetrates rather deeply into most tissue. In fact, careful control of the laser dose shows that radiation distribution is dominated by scattering in this wavelength range (59). If spectrally adapted chromphores are introduced and selectively retained in specific cellular sites, narrow-band irradiation can trigger selective photochemical reactions in vivo with subsequent photobiological transformations; hence, energy can selectively be delivered to deep target cells. Normal processes such as melanogenesis can thus be photoactivated in vitiligo Psoralen Ultra-violet-A (PUVA) therapy. Photodamage to abnormal cells can also be induced such as photochemical modification of nucleic acids in psoriasis PUVA therapy by furocoumarins, or cytotoxic photosensitization therapy by haematoporphyrin in tumour cells.

A chromophore compound capable of causing light-induced reactions in molecules that do not absorb light may be called a 'photosensitizer' (9, 60). Following resonant excitation by a monochromatic source, the photosensitizer undergoes a series of simultaneous or sequential decays, which result in intramolecular transfer reactions and ultimately culminate in the release of highly reactive cytotoxic species, which cause irreversible oxidation of some essential cellular component and destroy the affected host tissues (61). The essence of photochemical interaction (which should, rather, be called *photosensitized oxidation*) lies in the 'assistance' of the exogenous chromophore receptor which acts as a photocatalyst: it is first activated by resonant absorption, thereby storing energy in one of its excited states; only when it deactivates can a reaction take place, but with a reactant that is not the photosensitizer.

Most photosensitizers currently used are organic dyes and therefore they exhibit the usual electronic structure of singlet states (total electron spin momentum $S=0$) and triplet excited states ($S=1$) where the triplet energy is accordingly smaller than the corresponding excited singlet state. Each electronic state is further subdivided into a large manifold of vibrational states.

The sequence of molecular reactions can be separated into several stages: excitation; decay; substrate reaction or reactant formation; and oxidation. With S as the sensitizer, the reaction kinetics can be schematically separated into two mechanisms which depend on substrate involvement in the crucial stage of reactant formation (62). Table 3 summarizes these pathways, and Fig. 4 shows the energy level diagram of a widely used sensitizer (HPD), the absorption spectrum of which is given in Fig. 2 (62).

Table 3. Photosensitization kinetics in Type I and Type II mechanisms, and possible carotenoid protection

Photosensitizer excitation	
Resonant excitation	
1. Singlet state absorption	$^1S + h\nu \longrightarrow {}^1S^*$
Decays	
2. Radiative decay (fluorescence)	$^1S^* \longrightarrow {}^1S + h\nu'$
3. Non-radiative singlet decay	$^1S^* \longrightarrow {}^1S$
4. Intersystem crossing	$^1S^* \longrightarrow {}^3S^*$
5. Triplet state decay	$^3S^* \longrightarrow {}^1S$
6. Triplet phosphorescence decay	$^3S^* \longrightarrow {}^1S + h\nu''$
Type I mechanisms	
Free radical derivations	
7. Hydrogen transfer	$^3S^* + RH \longrightarrow SH^{\cdot} + R^{\cdot}$
8. Electron transfer	$^3S^* + RH \longrightarrow S^{\cdot -} + RH^{\cdot +}$
Reactant formations	
9. Hydrogen dioxide	$SH^{\cdot} + {}^3O_2 \longrightarrow {}^1S + HO_2^{\cdot}$
10. Superoxide anion	$S^{\cdot -} + {}^3O_2 \longrightarrow {}^1S + O_2^{\cdot}$
Oxidation	
Type II mechanisms	
Reactant formation	
7. Intermolecular exchange	$^3S^* + {}^3O_2 \longrightarrow {}^1S + {}^1O_2^*$
Oxidation	
8. Cellular oxidation	$^1O_2^* + X \longrightarrow X(O)$
Carotenoid protection	
1. Singlet oxygen extinction	$^1O_2^* + CAR \longrightarrow {}^3O_2 + {}^3CAR$

^1S, ground singlet state of sensitizer; $^1S^*$, excited singlet state of sensitizer; $^3S^*$, excited triplet state of sensitizer; $^3O_2$, ground triplet state of oxygen; $^1O_2^*$, excited singlet state of oxygen; RH, substrate; X, cellular target; X(O), oxidized cellular target; CAR, carotenoid.

Of the electronically excited derivatives of the photosensitizer, the excited triplet state $^3S^*$ is generally endowed with the greatest reactivity because of its favourable spin configuration: furthermore, its relatively long lifetime (1 ms to a few seconds), when compared to the $^1S^*$ fluorescence lifetime (0.1–100 ns, depending on the solvent), increases its probability of interacting with other molecules (62). A prerequisite for efficient photodynamic sensitizers is that they possess a high quantum yield η of intersystem crossing: the usual value ($\eta \sim 10^{-3}$), which is small when compared to the fluorescence yield, is often the rate-limiting factor (15).

In the Type I mechanism the $^3S^*$ species are involved directly with the substrate from which neutral or charged free radicals are derived, giving rise to a wide variety of possible further reactions: e.g. promotion of chain processes by interaction with other substrate targets, or reactions with oxygen to yield peroxidized products that attack the substrate.

In the Type II mechanism, the $^3S^*$ species are involved in transfer reactions to molecular oxygen (triplet $^3O_2$ ground state) which is promoted to its singlet state $^1O_2^*$ (first electronic excited state at 7900 cm^{-1}). The reaction between $^3S^*$ and $^3O_2$ corresponds to an electronic exchange collision with a spin rearrangement which is all the more probable because it is a quasi-resonant interaction without a net change of spin (J.L. Boulnois, unpublished observations). Owing to its peculiar electronic orbital and spin configuration, $^1O_2^*$ is highly electrophilic: it efficiently oxidizes electron-rich sites in neighbouring biomolecular targets. It is believed that target sites are proteins, nucleic acids and mitochondria, presumably located on cell membranes (61, 62). Singlet oxygen lifetimes are rather long, ranging from 5 to 50 μs in most solvents, with a ten-fold increase in deuterated solvents. Consequently, the limited diffusion length of $^1O_2^*$ maintains selectivity on a cellular basis. In fact, this *photodynamic action*, in which molecular oxygen is consumed in a photosensitization reaction, has been known by chemists and biologists alike for more than 50 years (9, 63).

In general both types of mechanism may occur competitively, the efficiency of either

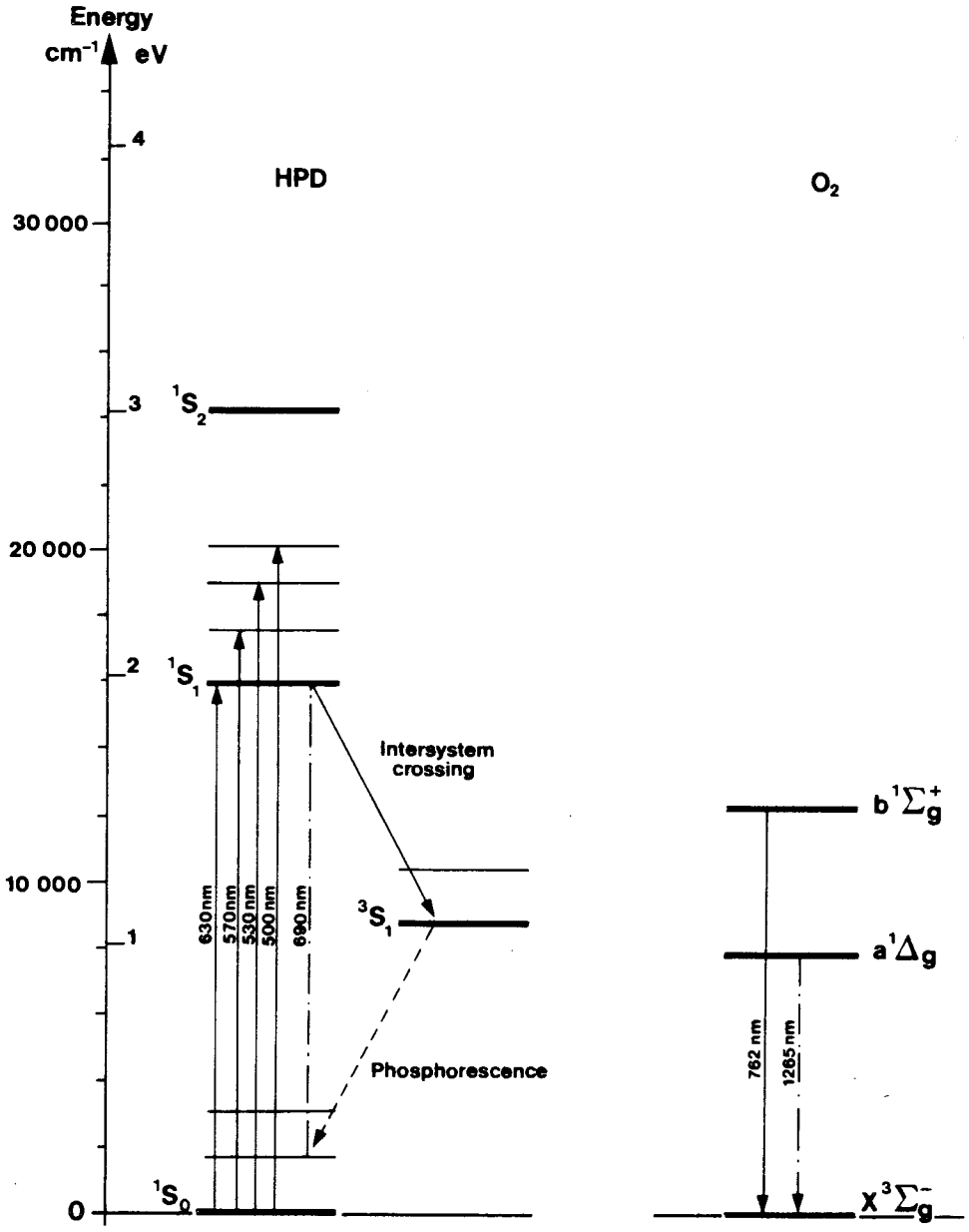

Fig. 4. Energy level diagrams of haematoporphyrin derivative (HPD) and molecular oxygen.

mechanism being controlled by the nature of S, by the relative concentration of oxygen and substrate, and by rate constants for the substrate–sensitizer and oxygen–sensitizer interactions. Since O_2 is much less soluble in water than in most organic solvents, decreasing the solvent polarity can be expected to favour Type II sequences; on the other hand, the complexation of the sensitizer with the substrate prior to irradiation, which often takes place in biological systems, enhances the probability of Type I mechanisms (64). For completeness, it should be mentioned that two-photon laser production of porphyrin radicals has been recently demonstrated to be highly effective (65).

Several points can be made about the efficacy of photosensitized oxidation. First, the photosensitizer is a 'true' photocatalyst since it is generally not consumed and is returned to its singlet ground state ^1S (62, J.L. Boulnois, unpublished observations). Second, all decays at one point or another, whether from singlet or triplet states, involve inelastic processes, sometimes with large cross-sections, all yielding a vibrational excited state of the ^1S ground state with efficient coupling to the surrounding thermal heat bath; even radiative processes

Table 4. Physical principles of photodynamic therapy

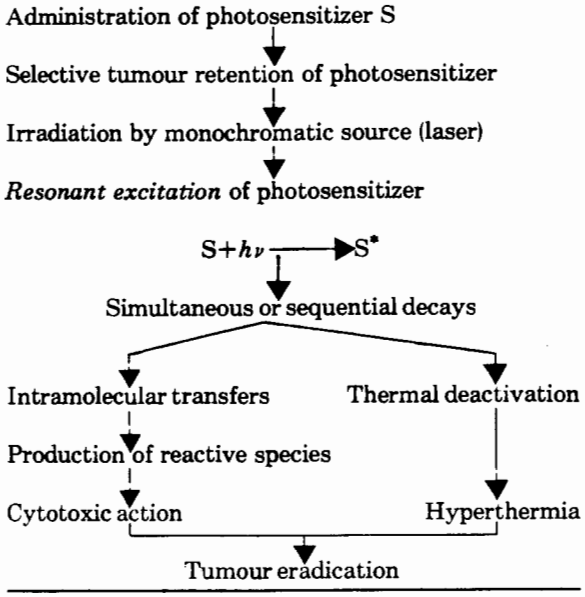

participate ($\nu' < \nu$ or $\nu'' < \nu$) and therefore contribute to heat generation in the bulk.

Owing to its selective targeting, this mode of action is attractive in photodynamic therapy (10, 11). A summary of the photophysical steps involved in this therapeutic procedure is given in Table 4. Current experimental approaches to cancer management rely on the selective retention of haematoporphyrin derivative (HPD) in malignant tissue. Several photosensitizers have long been known, such as fluorescein, berberin sulphate, tetracycline, but certain ones have been found to have a higher affinity for tumour cells than for healthy ones, among which are HPD, DHE (dihaematoporphyrin ether) (66), and certain groups of phthalocyanins (67). HPD, a mixture of products obtained from haematoporphyrin stabilized by acetic and sulphuric acids, seems to be the most suitable for clinical use primarily because of its selective retention in the tumour and its attractive absorption peak at 630 nm; HPD kinetics have been characterized by picosecond fluorescence spectroscopy in phosphate-buffered saline, yielding measurements of fluorescence lifetime (~ 240 ps) and radiationless transition rate (~ $4\times10^{9}s^{-1}$) (68). DHE has also been shown recently to be potentially useful since it appears to be twice more active than HPD and it has a strong tendency for self-association (66).

It is important to stress that during the weeks following photodynamic therapy with HPD it would be possible to protect patients by using the natural green plant or photosynthetic bacteria protector, namely the carotenoids: these agents protect photosynthetic systems against photosensitization by their own chlorophyll (69). Their molecular protection mechanism is a complete reversal of the singlet oxygen formation, and consists in $^{1}O_{2}^{*}$ quasi-resonant extinction, which produces the non-toxic triplet state of carotenoids ^{3}CAR, which deactivate rapidly (see Table 3). This photoprotective property of carotenoids has been successfully tested in a therapy against erythropoietic protoporphyria (70).

In view of the rather long irradiation times for photodynamic therapy (typically 1000 s), a basic question may be asked about the photochemical process: could the power density be significantly raised and the interaction time reduced? Owing to the small quantum yield, the number of molecules directly decaying towards the ground state is at least 10^{3} times larger than the number involved in singlet oxygen production. In c.w. irradiation, a large thermal component is thus associated with the process and only at low power densities can this excess heat be dissipated so that the photodynamic effect remains dominant. The situation is, of course, different in pulse configurations; photodynamic therapies are investigated on 100 ns time-scales, with metal vapour lasers, in which the pulse repetition rates are adjusted to the characteristic thermal relaxation time of the irradiated tissue (71).

Another point to consider is the use of a monochromatic source for irradiation. Currently the technique relies on argon-pumped continuous wave dye lasers which emit about 1 W at 630 nm, but a white light-source such as a xenon lamp with an appropriate filter (~10 nm) would perform similarly. Although they are not adequate for large surface treatments, lasers offer the advantage of high power densities which may reduce treatment times in localized areas since the question is one of dosimetry (15, 59); however, their major attraction stems from their ease of coupling to fibre-optic systems. Irradiation at the appropriate wavelength (514 nm for superficial tumours and 630 nm for deeper lesions) with energy doses ranging between 10 and 100 J/cm^{2}, results in tumour eradication. Current systems may not provide the best medical laser combination, and a single powerful source might be preferable. High-repetition-rate (3 to 5 kHz) metal vapour lasers, such as copper (λ=510 nm, 578 nm), gold (628 nm), manganese (534 nm) or lead (723 nm) may supersede current systems, since they offer very

high average power in the visible range (up to 20 W) with potentially simpler designs: coupled to slow scanning devices, they could thus facilitate treatment of large areas with little thermal component.

Recent measurements have shown that the increase in tissue temperature induced by photodynamic therapy could contribute to cell destruction (72). Such a role for hyperthermia in enhancing tumour control has been tested by monitoring sequential photodynamic treatments and localized microwave irradiation in vivo (73). The origin of this hyperthermic component in photodynamic therapy is naturally linked to the efficient decays of the excited singlet state $^1S^*$: an increase in tissue temperature to the 45 °C range may prove to be a useful alternative owing to the large induced death of tumour cells.

The effectiveness of extremely low-intensity laser irradiation (power 1–5 mW) on biological tissue has been the subject of controversial claims. In particular, clinical investigation has covered the so-called wound healing or anti-inflammatory properties of red light or near infrared sources such as He-Ne lasers (74, 75), or GaAs laser diodes, and the possible stimulation of microcirculatory effects and other features. Typical energy doses ranged from 1 to 10 J/cm^2. Presumably, observers have noticed improvements but reasonable explanations based on systematic experimental protocols have yet to be proposed. However, the stimulation of DNA synthesis has been studied (76), and recently the activation of the enzyme–substrate complex and transformations of prostaglandins have been reported but not unequivocally established (77). In all cases the controversy stems from the difficulty in specifying the photochemical channels of the reactions involved. Detailed investigations in this area are badly needed.

Electro-mechanical interaction

In this mode of interaction, a fluence of about 100 J/cm^2 is delivered to possibly transparent tissues by an Nd-YAG laser in extremely short time exposures by means of either mode-locked 30 ps pulses or 10 ns Q-switched pulses. The process is not maintained by linear absorption and is consequently not thermal.

Rather, the high-peak-power laser pulse, when focused at a target, creates high irradiances (approximately 10^{10} W/cm^2 for ns pulses and 10^{12} W/cm^2 for ps pulses) which locally generate high electric fields (10^6–10^7 V/cm) comparable to average atomic or intramolecular Coulomb electric fields; such large fields induce a dielectric breakdown of the target material resulting in the formation of a microplasma, i.e. an ionized volume with a very large free electron density. The shock wave associated with the plasma expansion generates a localized mechanical rupture for spatial extensions where the pressure rise is superior to the yield strength of encountered tissue (78). Table 5 summarizes the overall sequence of physical processes involved.

Table 5. Physical principles of laser-induced breakdown

• Short laser pulse focused at target	$I \sim \frac{(E_p/\tau_p)}{w_s^2}$
↓	
• High power density	$I \sim 10^{12}$ W/cm^2
• High electric field	$E = \left(\frac{2I}{c\epsilon_0}\right)^{\frac{1}{2}} \sim 10^6$ V/cm
↓	
• Dielectric breakdown (multiphoton process)	$E_{laser} \sim E_{\substack{ionization \\ molecules}}$
↓	
• Plasma formation Free electrons	$N_e \sim 10^{21}$/cm^3; $T > 20\,000$ °C
↓	
• Spherical shock wave propagating at sound velocity	P (bars) $\sim 13 E_p/R^3$; E_p(mJ); $A \sim 15 \times 10^6$ mm/s r(mm)
↓	
• Localized mechanical rupture for small radius	$P >$ yield strength of tissues

N_e, electron number density; τ_p, pulse duration; A, shock wave velocity; w_s, spot radius.

At the microscopic level, the mechanism responsible for optical breakdown is the massive generation of free electrons. It is possible to distinguish the initiation, which corresponds to a localized electron 'seeding' by ionization involving a few electrons only, from the massive subsequent electron photoproduction.

In the initial phase, the ionization mechanisms, in which energies of about 7 to 10 eV must be supplied to bound electrons to separate them from individual molecules, differ depending on pulse duration (78, 79). For Q-switched pulses (3 to 10 ns duration), ionization is caused by thermionic emission resulting from

focal heating of the target, where local 'temperatures' (i.e. specific molecular energies) exceeding several tens of thousands of degrees are reached, all the more rapidly when impurities are present. For very short mode-locked 20 ps pulse trains, molecular ionization is obtained by a non-linear process called multiple photon absorption: because of the extremely high irradiance at the focal spot, photons can add up their energies coherently and provide the ionization energy that produces free electrons.

The threshold for optical breakdown is higher for mode-locked ps pulses than for Q-switched ns pulses: in air, the threshold for a single 25 ps pulse is about 10^{14} W/cm^2 whereas it is only 10^{11} W/cm^2 for a 10 ns pulse (79). In biological solutions, these numbers are reduced by a factor of 100, the total energy density delivered in achieving optical breakdown (~10 J/cm^2) being ultimately the same for a mode-locked pulse train and a Q-switched pulse, even though peak power density is, on average, 100 times higher for ps pulses (80).

The key physical element of the electromechanical mode of interaction is rooted in the massive subsequent photoproduction of extraneous free electrons. The process is termed 'electron avalanche growth' or 'inverse Bremstrahlung effect' (18). In the field of molecules or ions, free electrons already seeded absorb incoming photons and convert this energy into kinetic energy, thereby increasing their velocity: on colliding with neighbouring molecules, rapid free electrons ionize collision partners when their relative kinetic energy is sufficient and, hence, this process creates extraneous free electrons.

The detailed microscopic process is basically a free–free absorption (i.e. a transition in which a free electron is present in the initial and final states) which must necessarily take place in the field of an ion A^+ or in that of a neutral atom. This process can be schematically written:

$$h\nu + e + A^+ \longrightarrow e + A^+$$

The particularly important feature of this process is that there is no restriction of the photon energy: in fact the cross-section is largest for small photon energy $h\nu$, which corresponds to an extremely large efficiency of the inverse Bremstrahlung effect (18). Each electron in turn absorbs more photons, accelerates, strikes more atoms or molecules and ionizes them in an avalanche process with exponential growth: in a few hundred picoseconds a very large free electron density (typically 10^{21}cm^{-3}) is thus created in the focal volume of the pulsed laser beam. This is called laser-induced breakdown of the dielectric medium.

The condition for plasma growth and sustainment is that losses such as inelastic collisions or free electron diffusion do not quench the inverse Bremstrahlung avalanche (81, 82). A general macroscopic model which encompasses creation and loss mechanisms, and which predicts the temporal evolution of all geometric and thermodynamic parameters can be constructed (83, J.L. Boulnois, unpublished observations). Fig. 5 represents on a logarithmic time-scale the typical evolutions of the principal macroscopic parameters (plasma radius, electron number density and pressure) following irradiation by a 25 ps pulse. If the rise time is sufficiently short, irrespective of pulse duration, a permanent state is reached in about 100 ps or less: the origin is the so-called 'plasma shielding effect'. As the plasma number density N_e increases, the characteristic plasma frequency ω_p, proportional to $N_e^{\frac{1}{2}}$, increases, and so does photon scattering. Consequently, progressively less energy is coupled from the laser field to free electrons; the critical density N_e^* at which incident energy is not converted any further is obtained when the plasma frequency ω_p becomes equal to the pulsation ω of the incident electromagnetic wave (84): in terms of the radiation wavelength, this condition is written:

$$N_e^* \leqslant \frac{\pi}{\lambda^2 r_0}$$

Here r_0 is the classical electron radius (2.8×10^{-13} cm): for Nd-YAG laser radiation, the upper bound electron density is $N_e^* \sim 10^{21}$ cm^{-3}. When this density is reached (in less than 100 ps with a 25 ps pulse), the plasma radius is about 50 μm, and pressure and temperature have reached their maxima. As the plasma shock wave expands, it cools, and the pressure falls accordingly. For a mode-locked picosecond pulse train with pulses typically separated by 7 ns intervals, the cooling rate between pulses is faster than with Q-switched nanosecond pulses, since N_e remains approximately constant throughout the exposure time, but the process is qualitatively similar.

In the permanent regime, once the critical density N_e^* has been reached, the plasma expansion problem is quite similar to the well known 'strong explosion in a homogeneous medium' with constant density ϱ_0 (85). At time t the wave reaches a radius R and encompasses a volume whose mass is $4\pi R^3\varrho_0/3$; assuming an instan-

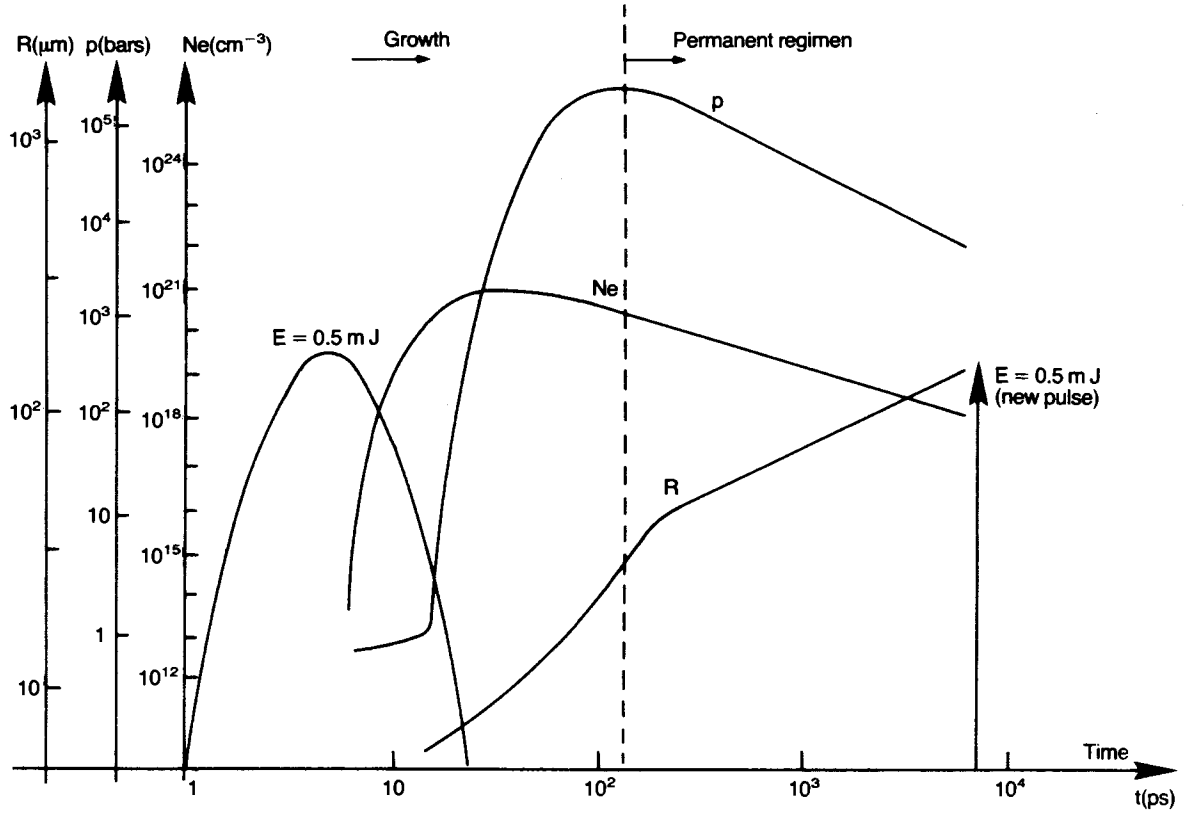

Fig. 5. Temporal evolution of plasma parameters (electron number density N_e, plasma radius R, and pressure p), following a laser-induced breakdown with 0.5 mJ energy in a 25 ps pulse (J.L. Boulnois, unpublished observations).

taneous release of an energy amount E, the wave expands *adiabatically* and the pressure behind this shock wave is proportional to the average energy per unit volume $p \sim E/R^3$. It is then quite simple to verify that the shock-front velocity is proportional to $R^{-3/2}$, and from there to check that the front radius time evolution is $R \sim (E/\varrho_0)^{1/5}t^{2/5}$, whereas for pressure $p \sim (E/\varrho_0)^{2/5}t^{-6/5}$. These results closely match the data in Fig. 5 for times greater than 100 ps. Such temporal scaling laws are essential for predicting the limits of plasma expansion and for modelling the spatial extent of injury. Clearly, inside the spherical volume where the pressure is superior to the yield strength of biological structures encountered, a localized mechanical rupture will take place, resulting in an opening or disruption of these structures: this is the physical basis of new ophthalmic surgical techniques (12).

The plasma shielding effect, mentioned above, is very important in retinal protection during pulsed Nd-YAG laser ophthalmic treatments in the anterior segment of the eye. Published work confirms the current considerable confusion about the role of plasma as a shield to protect the retina (80, 86). The real question is: in how short a time is the critical plasma electron number density N_e^* reached?

First, it should be recalled that when the plasma is highly ionized, the absorption coefficient, being proportional to N_e^2, is very large, typically in the range 1–10 cm^{-1} (87); consequently, one should expect a large absorption of the incident beam. In the case of picosecond mode-locked pulse trains, a typical 25 ps pulse contains about 3×10^{15} photons which are absorbed in less than 1 μm because the growth rate of N_e is extremely large, about $10^{31}\,s^{-1}$ as seen in Fig. 5: hence the fraction of incident energy transmitted to the retina is small during optical breakdown, the same sequence of processes being reproduced 7 ns later. For Q-switched nanosecond pulses, the answer to the question depends fundamentally on the pulse rise time: if the rise time is of the order of 100 ps, then the process is quite similar to that for picosecond pulses, but if the rise time is longer (~1 ns) then significant energy transmission is possible because the growth rate of N_e is not sufficient to ensure strong absorption and to overcome scattering of the incident photon flux

(J.L. Boulnois, unpublished observations). It should be noticed that by coincidence, 100 ps is approximately the time during which light travels the distance from the eye's anterior segment to the retina. Practical prevention of retinal injury in the course of intraocular surgery is achieved by magnifying the laser beam and then focusing with a short focal lens: with a sufficiently large converging cone angle, irradiance decreases rapidly beyond the focal point owing to the increased area of exposed surface.

This photodisruption process is of particular interest in several pathological conditions of the eye for the non-invasive treatment of capsulotomies (12, 88, 89), certain iridectomies, the removal of vitreous strands or the dissociation of opacified membranes which frequently develop after cataract surgery. Since this technique is simple it can be used in ambulatory treatments. Recently, optical breakdown techniques have been used also in cardiovascular models (90) to investigate possible disintegrations of atheromatous plaques in small arteries by the use of pulsed photodisruption. Although promising preliminary results in vitro suggest that this technique is feasible, a main difficulty remaining is the transport within fibres of the necessary high peak powers if the model is to be of any future therapeutic interest.

Photoablative interaction

As already stated, u.v. radiation is extremely strongly absorbed by most biological molecules (see Fig. 2) in a band between 200 and 360 nm: absorption coefficients as large as $10^4\,cm^{-1}$ are common and absorption depths are consequently very small, a few μm at most.

This feature has recently been exploited experimentally to produce well defined, non-necrotic photoablative cuts of very small width (~50 μm) by exposure to excimer lasers at several u.v. wavelengths (ArF: 193 nm/6.4e V; KrF: 248 nm/5 eV; XeCl: 308 nm/4 eV), with short pulses (~10 ns) focused on tissue (~$10^8\,W/cm^2$) (13, 14, W.S. Grundfest et al, unpublished observations). Similar sharp cuts (2–3 μm) with minimal thermal damage are also obtained with the fourth harmonic of the Nd-YAG laser at 266 nm (4.7 eV); the excellent cutting quality is due to the high spatial quality of the beam (91). Control of thermal damage is clinically important since it generally produces undesirable biological effects.

Ablation of material with u.v. lasers has been well investigated in polymer films used as photoresists in semi-conductor processing (92, 93) and takes place at well defined wavelength-dependent fluence thresholds related to the absorption cross-section of the polymer constituents. Recently, systematic ultrastructural explorations of the etched substrate and chemical analysis of the effluent have been done in a comparative study between a synthetic polymer and bovine cornea in vitro; remarkably similar u.v. photoreactions in both materials have been attributed to the similarity of their respective polymeric structure.

The photoablative process consists in a photodissociation, i.e. the direct breaking of intramolecular bonds in polymeric chains, caused by absorption of incoming photons, followed by effluent desorption: in the photon energy range of 5–7 eV, biopolymers such as collagen may dissociate by absorption of a single photon. The microscopic mechanisms correspond to transitions of a macromolecule AB that is promoted to a repulsive electronic state that yields photoproducts A and B. This can be written:

$$h\nu + AB \longrightarrow A + B$$

What is the probability of such a process taking place? For typical photon energies around 6 eV, absorption cross-sections for organic polymers are rather small ($10^{-18}\,cm^2$), but electronic transitions that satisfy the Franck-Condon principle are known to be significantly favoured (18). One further problem concerns the fate of molecular photofragments: how do they leave the surface? It is currently assumed that desorption is an important secondary mechanism, but the dynamics of nuclear motion are not yet clearly ascertained. However, radiative dissociation in repulsive electronic excited states yields products whose kinetic energy is necessarily the difference between $h\nu$ and the bound-state molecular energy; not every excited state may achieve photodissociation and a quantum yield η is thus associated with the process.

The chemical structures of both collagen and the organic polymer polymethyl methacrylate (PMMA) contain monomer units of the same average molecular weight (100) with one chromophoric group per monomer. Measurements of the etch depth per pulse in bovine cornea and in PMMA show remarkably similar behaviour as a function of fluence (94). Nearly identical etch thresholds are obtained with both materials, the photofragments being methyl methacrylate (MMA) and, presumably, amides or peptides

from the polypeptic triple helix of procollagen. With increasing fluence, a steeply rising photoproduction is observed and a saturation reached when recombination rates overtake photodissociation rates: u.v. absorption at 193 nm being at least tenfold stronger than at 248 nm, etch depths per pulse are inversely proportional as expected (~ 0.5 μm and 5 μm respectively). Saturation is achieved at nearly 0.3 J/cm^2 fluence for 193 nm irradiation and at 3 J/cm^2 for 248 nm, when the photon per monomer ratio reaches unity (94). For a monomer with a molecular weight of 100, this limit corresponds to an ablated mass nearly equal to 2×10^{-4} g per Joule: this is totally consistent with quantum yield measurements, which give approximately 2.4×10^{-4} g/J for MMA and bovine cornea photofragments, irrespective of wavelength (94).

Such comparative studies unravel some essential steps in photoablative processes. Laser-induced photodissociation is an extremely rich field: a comprehensive photophysical analysis for polyatomic molecules would have to consider how structured is their vibrational manifold, whether the process is single photon or multiphoton, whether it is resonant or non-resonant, whether the incoming field is weak or strong and whether it is single mode or multimode (95). One can thus anticipate that u.v. photodissociation, when applied to biomolecules, will prove to be even more complex.

Recalling the characteristic relaxation times given in Table 2, we notice that u.v. photoablation is inherently limited by pulse width. The limitation is determined either by characteristic de-excitation times, of the order of 100 ns at most, arising from recombination, attachment or other quenching mechanisms, or it is determined by water thermal diffusion occurring on a 30 μs time-scale. Long u.v. exposures would, hence, be associated with a large thermal component; this explains the position of the photoablative interaction family in Fig. 1.

When validated, this experimental surgical technique may prove to be unique in its ability to produce sharp incisions with minimal thermal damage to adjacent normal structures. Table 6 summarizes the pathways of the processes involved. Photoablative techniques with excimer lasers have been applied to various microsurgical models such as skin removal (14) and ablation of atheromatous plaques in human vascular tissue in vitro (W.S. Grundfest et al, unpublished observations). But a promising area appears in the treatment of several ocular disorders because of the potential

Table 6. Physical principles of laser photoablation

Short u.v. laser pulse (10 ns) focused on tissue	I ~10^8 W/cm^2
↓	
Strong absorption in the u.v. (6eV) (proteins; amides; peptides)	Absorption depth ~ 1 μm
↓	
Promotion to repulsive excited state	
↓	
Photodissociation	
↓	
Desorption	
↓	
No necrosis	

of changing the eye's refractive power (e.g. reducing myopia) by making radial corneal incisions. Ablation of corneal stroma with 193 nm radiation seems to produce most precise cuts, as narrow as 20 μm, without the ragged edges produced at 248 nm (13). Such an effect might be attributed to the difference in absorption (α=2700 cm^{-1} at 193 nm; but α=210 cm^{-1} at 248 nm). However, beam quality might also be crucial, as suggested by the 3 μm cuts achieved with the fourth harmonic of an Nd-YAG laser (91). Further investigations are in progress, in particular to answer questions about possible mutagenic or carcinogenic effects in the interaction with DNA in neighbouring cells; this is of the utmost importance because, in vivo, u.v. photochemistry may not only alter DNA bases but may also modify RNA structure photochemically, as well as enzymic proteins and perhaps membranes; hence it may eventually change cell functions. Further work is needed to demonstrate whether photoablative techniques might become useful as microsurgical tools.

CONCLUSION

A comprehensive analysis and comparison is presented of different biomedical applications for lasers. The photophysical steps of the processes involved have been emphasized. Four groups of interactions may be distinguished according to their radically different tissue reactions, which depend on the duration of irradiation: the proposed argument is based on the magnitude of the energy dose supplied, which has been shown empirically to be *approximately constant* in all instances, over more than 12

decades of time. Absorption characteristics of primary absorbers, kinetics, and associated relaxation times have been analysed for each group, and they support the proposal. This review of the relatively young fields of laser photodynamic therapy, pulsed lasers in the breakdown mode, or u.v. photoablative techniques has attempted to demonstrate the versatile potential that lasers may offer in photomedicine in the near future. More innovations are likely to come, but one cannot hold an unbridled optimism about the immediate applications. The complexity of the problems encountered underlines the need for careful evaluation of results before instruments become accepted in an operational clinical environment.

ACKNOWLEDGEMENTS

The author is indebted to Professor R. Sultan, Rueil-Malmaison Hospital, who suggested an invited paper at the Second International Congress of the European Laser Association, Brussels, January 1985: his keen arguments were particularly stimulating.

REFERENCES

1 Goldman L, Rockwell J, Jr. *Lasers in Medicine*. New York: Gordon and Breach, 1971
2 Adey WR. Tissue interactions with nonionizing electromagnetic radiation. *Physiol Rev* 1981, 61:435
3 Hayes JR, Wolbharsht ML. Models in pathology — mechanisms of action of laser energy with biological tissues. In: Wolbharsht ML (ed) *Laser Applications in Medicine and Biology*, Vol 1. New York: Plenum, 1975: Chap 1
4 Pratesi R, Sacchi CA (eds) *Lasers in Photomedicine and Photobiology*, New York: Springer, 1980
5 Regan JD, Parrish JA. *Science of Photomedicine*. New York: Plenum, 1982
6 Grandolfo M, Michaelson SM, Rindi A (eds) *Biological Effects and Dosimetry of Nonionizing Radiation*. New York: Plenum, 1983
7 Parrish JA, Deutsch JF. Laser photomedicine. *IEEE (Inst Electr Electron Eng) J Quantum Electron* QE 20 1984, 12:1386
8 Kaplan I (ed) *Laser Surgery*. Jerusalem: Academic, 1976
9 Spikes JD, Straight R. Sensitized photochemical processes in biological systems. *Annu Rev Phys Chem* 1967, 18:409
10 Diamond I, Granelli S, McDonaugh AF. Photodynamic therapy of malignant tumours. *Lancet* 1973, ii:1177
11 Dougherty TJ. Photoradiation therapy. Abstr Am Chem Soc Mtg, Chicago Il, September 1973:No 014
12 Aron-Rosa D, Aron J, Griesemann J, Thyzel R. Use of the Nd:YAG laser to open the posterior capsule after lens implant surgery. *J Am Introcul Implant Soc* 1980, 6:352
13 Trokel SL, Srinivasan R, Braren B. Excimer laser surgery of the cornea. *J Ophthalmol* 1983, 96:710
14 Lane RJ, Linsker R, Wynne JJ et al. Ultraviolet-laser ablation of the skin. *Lasers Surg Med* 1984 4:201
15 Boulnois JL. A general classification of laser-tissue interactions. *Lasers Surg Med* 1985:in press
16 Giese AC (ed) *Photophysiology*, Vol 6. New York: Academic, 1971
17 Smith KC. Photobiology of ultraviolet radiation. In: Pratesi R, Sacchi CA (eds) *Lasers in Photomedicine and Photobiology*. New York: Springer, 1980
18 Bond JW, Watson KM, Welch JA. In: *Atomic Theory of Gas Dynamics*. Massachussets: Addison-Wesley Reading, 1965
19 Parrish JA. New concepts in therapeutic photomedicine: photochemistry, optical targeting and the therapeutic window; *J Invest Dermatol* 1981, 77:45
20 Brunetaud JM, Mordon S, Bourez J et al. Therapeutic applications of lasers. *Optical Fibers in the Biomedical Field (Proc SPIE* 405) May 1985:2
21 van Gemert MC, Schets GA, Stassen EG, Bonnier JJ. Modelling of coronary laser angioplasty. *Lasers Surg Med* 1985 5:219
22 van Gemert MC, de Kleijn WJ, Hulsbergen JP. Temperature behavior of a model portwine stain during argon laser coagulation. *Phys Med Biol* 1982, 27:1104
23 Welch AJ. The thermal response of laser-irradiated tissue. *IEEE (Inst Elec Electron Eng) J Quantum Electron* QE 20 1984, 12:1471
24 Mordon S, Brunetaud JM, Mosquet L et al. Effets thermiques des lasers: étude par camera thermique infrarouge. *Laser Médical*. Opto 82. Paris: Masson 1984:58
25 L'Espérance FA. *Ocular photocoagulation*. Saint-Louis: Mosby, 1975
26 Little HL, Zweng HC, Peabody RR. Argon laser slit lamp retinal photocoagulation. *Trans Am Acad Ophthalmol Oto-Laryngol* 1970 74:85
27 Coscas G. Le laser à krypton en ophtalmologie: premiers essais expérimentaux et cliniques. *Bull Mem Soc Fr Ophtalmol* 1981, 87:100
28 Karduck B, Richter MG, Blank M. Laserchirurgie des Stimmbandes. *Laryngol Rhinol Otol* 1978, 57:419
29 Frêche C, Lotteau J, Abitbol J. Le laser en O.R.L. *Concours Med* 1979:2607
30 Toaff R. The CO_2 laser in gynecological surgery. In: Kaplan I (ed) *Laser Surgery*. Jerusalem: Academic 1976
31 Kiefhaber P, Nath G, Moritz K. Endoscopical control of massive gastrointestinal hemorrhage by irradiation with a high-power neodymium-YAG laser. *Prog Surg* 1977: 140
32 Grotelüschen NB, Reilmann M, Bödecker V, Buchholz J. A high power Nd:YAG laser as a cutting tool in experimental surgery. In: Kaplan I (ed) *Laser Surgery*. Jerusalem: Academic 1976:167
33 Godlewski G, Miro L, Chevalier JM, Bureau JP. Experimental comparative study on morphological effects of different lasers on the liver. *Res Exp Med* 1982, 180:51
34 Bown SG, Salmon PR, Storey DW et al. Nd:YAG laser photocoagulation in the dog stomach. *Gut* 1980, 21:818
35 Stachler G, Hofstetter A, Gorisch W et al. Endoscopy in experimental urology using argon-laser-beam. *Endoscopy* 1976, 8:1
36 Toty L, Personne C, Colchen A, Vourc'h G. Bronchoscopic management of tracheal lesions using the Nd:YAG laser. *Thorax* 1981, 36:175
37 Nims TA, McCaughan JS. Clinical experience with CO_2 laser vaporisation of neoplasm. *Lasers Surg Med* 1983, 3:265

38 Oshiro T. In: Oshiro T (ed) *Laser treatments for nevi.* Med Laser Res Co Ltd. Tokyo: Fukuin Printing Co, 1980

39 Carruth JAS. The minimal blanching power technique for the treatment of portwine stains with argon lasers. In: The Medical Laser. Present and Future. Second International Congress European Laser Association, Brussels, January 1985

40 Deutsch TF, Oseroff AR. New medical uses of lasers: a survey. Proc CLEO Baltimore, 1985:paper WF3

41 Macruz R, Martins JR, Tupinamba A et al. Therapeutic possibilities of laser beams in atheromas. *Arq Bras Cardiol* 1980, **34**:9

42 Choy DS, Sterzer SH, Rotterdam HZ et al. Transluminal laser catheter angioplasty. *Am J Cardiol* 1982, **50**:1206

43 Ginsburg R, Kim DS, Guthaner D et al. Salvage of an ischemic limb by laser angioplasty: description of a new technique. *Clin Cardiol* 1984, **7**:54

44 Abela GS, Cohen D, Feldman RL et al. Use of laser radiation to recanalize arteries in live rabbits. *Clin Res* 1983, **31**:458A

45 Case RB, Choy DS, Dwyer EM, Silvernail PJ. Absence of distal emboli during in vivo laser recanalization. *Lasers Surg Med* 1985, **5**:281

46 Geschwind H, Boussignac G, Tesseire B et al. Percutaneous transluminal laser angioplasty in man. *Lancet* 1984, *i*:844

47 van Gemert M, Verdaasdonk R, Stassen EG et al. Optical properties of human blood vessel wall and plaque. *Lasers Surg Med* 1985, **5**:235

48 Berns MW, Mirhoseini M (eds) Special issue: Laser applications to occlusive vascular disease. *Laser Surg Med* 1985, **5**:3

49 Neblett C. History and future of tissue welding. Proc Congress Laser Neurosurg III 1984:64 (abstr)

50 Jain KK, Gorisch W. Repair of small blood vessels with the ND:YAG laser: a preliminary report. *Surgery (St Louis)* 1979, **85**:684

51 Krueger RR, Almquist EE. Argon laser coagulation of blood for the anastomosis of small vessels. *Lasers Surg Med* 1985, **5**:55

52 Serure A, Withers WH, Thomsen S, Morris J. Comparison of carbon dioxide laser-assisted microvascular anastomosis and conventional microvascular sutured anastomosis. *Surg Forum* 1983, **34**:634

53 Lynne C, Carter M, Morris J et al. Laser-assisted vas anastomosis: a preliminary report. *Lasers Surg Med* 1983, **3**:261

54 Quingley MR, Bailes J, Kwaan HC et al. Microvascular anastomosis using the milliwatt CO_2 laser, *Lasers Surg Med* 1985, **5**:357

55 Tyrrell RM. *Photochem Photobiol Rev* 1977, **3**:35

56 Meyer HJ, Haverkampf K. Experimental study of partial liver resection with a combined CO_2 and Nd:YAG laser. *Lasers Surg Med* 1982, **2**:149

57 Sultan R, Fallouh H, Lefevre-Villardebo M, Ladouch-Badre A. The combined use of Nd:YAG and CO_2 lasers as a hemostatic knife in liver surgery. In: The Medical Laser: Present and Future. Second International Congress European Laser Association, Brussels, January 1985

58 *Lasers Appl* 1985, **4**:36, August

59 Svaasand LO, Doiron DR, Dougherty TJ. Temperature rise during photoradiation therapy of malignant tumors. *Med Phys* 1983 **10**:10

60 Dougherty TJ. Hematoporphyrin as a photosensitizer of tumors. *Photochem Photobiol* 1983, **38**:377

61 Weishaupt KR, Gomer CJ, Dougherty TJ. Identification of singlet oxygen as the cytotoxic agent in photoinactivation of a murine tumor. *Cancer Res* 1976, **36**:2316

62 Bensasson R. La photochimiothérapie par l'hématoporphyrine. Introduction, mécanismes moléculaires. In: *Laser Medical*, Opto 1982. Paris:Masson, 1984:29

63 Policard A. Etudes sur les aspects offerts par les tumeurs expérimentales à la lumière de Wood. *CR Seances Soc Biol Fil* 1924, **91**:1423

64 Jori G. The molecular biology of photodynamic action. In: Pratesi R, Sacchi CA (eds) *Lasers in Photomedicine and Photobiology*. New York: Springer 1980

65 Andreoni A, Cubeddu A, de Silvestri S et al. Two-step laser activation of hematoporphyrin derivative. *Chem Phys Lett* 1982, **88**:37

66 Dougherty TJ, Weishaupt KR, Boyle DG. Photodynamic therapy and cancer. In: DeVita VT et al (eds) *Principles and Practice of Oncology*. Philadelphia J.B. Lippincott, 1985

67 Moan J. Porphyrin-sensitized photodynamic inactivation of cells, a review. *Lasers Med Sci* 1986, 1:this volume

68 Yanmashita M, Sato T, Aizawa K, Kato H. Picosecond fluorescence spectroscopy of hematoporphyrin derivative and related porphyrins. In: Eisenthal KB et al (eds) *Picosecond phenomena III*. New York: Springer (*Springer Ser Chem Phys*) 1980:298

69 Krinsky NI. In: Isler O (ed) *Functions of carotenoids*. Basel: Birkhauser, 1971:669

70 Mathews-Roth MM. Beta-carotenotherapy for erythropoietic protoporphyria and other photosensivity diseases, In: Regan JD, Parrish JA (eds) *Science of Photomedicine* New York: Plenum, 1982

71 Cowled C, Grace, Forbes. Comparison of the efficacy of pulsed and cw red laser light in induction of phototoxicity by haematoporphyrin derivative. *Photochem Photobiol* 1984, **39**:115

72 Berns MW, Coffey J, Wile AG. Laser photoradiation therapy of cancer: possible role of hyperthermia. *Lasers Surg Med* 1984, **4**:87

73 Waldow SM, Henderson BW, Dougherty TJ. Enhanced tumor control following sequential treatments of photodynamic therapy and localized microwave hyperthermia in vivo. *Lasers Surg Med* 1984, **4**:79

74 Mester E. Laser application in promoting wound healing. In: Koebner MK (ed) *Lasers in Medicine*. Chichester: Wiley, 1980

75 Oraevskii AN, Pleshanov PG. Biochemical effect of laser radiation, *Sov J Quantum Electron* 1981, **12**:1593

76 Karu TI, Kalenko GS, Letokhov VS, Labko VV. Biological action of low-intensity visible light on HeLa cells as a function of the coherence, dose, wavelength, and irradiation regime. *Sov J Quantum Electron* 1982, **9**:1134 and 1983, **9**:1169

77 *Lasers Appl* 1985, **4**:36, March

78 Puliafito CA, Steinert RF. Short-pulsed Nd:YAG laser microsurgery of the eye: biophysical considerations. *IEEE (Inst Elect Electron Eng) J Quantum Electron* 20 1984, **12**:1442

79 Fradin DW, Bloembergen N, Letellier JP. Dependence of laser-induced breakdown field strength on plasma duration. *Appl Phys Lett* 1973, **22**:635

80 Steinert RF, Puliafito CA, Trokel S. Plasma formation and shielding by three Nd:YAG lasers. *Am J Ophthalmol* 1983 **96**:427

81 Smith DC, Haught AF. Energy-loss processes in optical

frequency gas breakdown. *Phys Rev Lett* 1966, 16:1085
82 Mitsak V, Saveskin V, Chernikiv V. Breakdown at optical frequencies in the presence of diffusion losses. *JETP Lett* 1966, 4:88
83 Krokhin ON. Generation of high-temperature vapors and plasmas by laser radiation. In: Arecchi FT, Schulz-du-Bois EO (eds) *Laser Handbook*, Vol 2. Amsterdam: North-Holland 1972: 1371
84 Smith DC, Meyerand RG. Laser radiation induced gas breakdown. In: Bekefi G (ed) *Principles of Laser Plasmas*. Chichester: Wiley, 1976: 457
85 Sedov LI. *Similarity and Dimensional Methods in Mechanics, Gostekhizadt*. 4th edn, Moskow, 1957 (English Translation, Holt M (ed) New York: Academic Press, 1959)
86 Steinert RF, Puliafito CA, Kittrell C. Plasma shielding by Q-switched and mode-locked ND:YAG lasers. *Ophthalmology* 1983, 90:1003
87 Bekefi G. Radiation Processes in Plasmas. New York: Wiley, 1966
88 Aron-Rosa D, Griesemann JC, Aron JJ. Use of a pulsed neodymium-YAG laser (picosecond) to open the posterior lens capsule in traumatic cataract: a preliminary report. *Surgery (St Louis)* 1981, 12:496
89 Fankhauser F, Roussel P, Steffen J et al. Clinical studies on the efficiency of high power laser radiation upon some structures of the anterior segment of the eye. *Int Ophthalmol* 1981, 3:129
90 Mayer G, Astier R, Englender J et al. Recanalization 'in-vitro' of atheromatous coronary arteries by short laser pulses. In: The Medical Laser: Present and Future. Second International Congress European Laser Association, Brussels January 1985
91 Berns MW, Gaster RN. Corneal incisions produced with the 4th harmonic (266 nm) of the Nd:YAG laser. *Lasers Surg Med* 1985, 5:371
92 Srinivasan R, Mayne-Benton V, Self-developing photoetching of polyethylene terephthalate films by far-ultraviolet excimer laser radiation. *Appl Phys Lett* 1982, 41:576
93 Deutsch TF, Geis MW. Self-developing UV photoresist using excimer laser exposure. *J Appl Phys* 1983, 54:7201
94 Srinivasan R, Braren B, Seeger D et al. Comparative study of the photochemistry and the cutting (etching) of a synthetix polymer and bovine cornea by excimer radiation. Proc CLEO Baltimore, 1985: paper WL2
95 Rahman NK. Laser-induced photodissociation. (Colloque C1 in Collisions in a Laser Field) *J Phys* 1985, 46:249

Key words: Photomedicine; Photobiology; Photoablative; Photochemical; Photothermal; Electromechanical; Lasers